Experimental evidence of monolayer arsenene: an exotic 2D semiconducting material

2D Materials

OPEN ACCESS

RECEIVED
8 July 2019

REVISED
5 November 2019

ACCEPTED FOR PUBLICATION
23 December 2019

PUBLISHED
5 February 2020

PAPER

Experimental evidence of monolayer arsenene: an exotic 2D semiconducting material

J Shah[1], W Wang[1,2], H M Sohail[1] and R I G Uhrberg[1]

[1] Department of Physics, Chemistry, and Biology, Linköping University, S-581 83 Linköping, Sweden
[2] MAX IV Laboratory, Lund University, Box 118, SE-221 00 Lund, Sweden

E-mail: jalil.shah@liu.se **(Experiment) and** weimin.wang@maxiv.lu.se **(Experiment and theory)**

Keywords: 2D material, ARPES, STM, DFT, arsenene

Abstract

Group V element analogues of graphene have attracted a lot of attention recently due to their semiconducting band structures and several other interesting properties predicted by theoretical investigations in the literature. In this study, we present atomic and electronic structure data of an arsenic (As) layer on Ag(1 1 1). Low-energy electron diffraction and scanning tunneling microscopy data provide evidence for an ordered layer with a lattice constant of 3.6 Å. This value fits with the theoretical range of 3.54–3.64 Å for buckled arsenene, which is the structure consistently predicted by various theoretical studies. The electronic structure obtained by angle-resolved photoelectron spectroscopy shows the existence of three 2D electron bands within 4 eV below the Fermi level. The number of bands and the agreement between experimental band dispersions and the theoretical band structure provide further evidence for the formation of monolayer buckled arsenene on Ag(1 1 1).

The isolation of 2D carbon in the form of a single-layer honeycomb structure (graphene) [1] was the starting point of the current intensive research on various 2D materials. In particular, the electronic properties, i.e. the high conductivity in combination with the linear dispersion of the π-band, forming a Dirac cone, are highly interesting for applications in nanoelectronics [2]. However, this utilization of graphene is severely hampered by the lack of an intrinsic band gap, which it shares with graphene-like structures of other group IV atoms, i.e. Si, Ge and Sn [3].

Layered materials formed by the group V atoms P, As, Sb and Bi, offer a possible solution to this problem. Theoretically, single-layer phosphorus (phosphorene) is predicted to have a direct band gap in the range 0.8–2.35 eV [4–8] depending on the calculation method. Experimental values for the optical and quasiparticle band gaps of 1.3 and 2.2 eV, respectively, were reported in [9], while a bandgap value of 2 eV has been reported from scanning tunneling spectroscopy measurements [6]. Experimental studies have been performed both on few-layer [9–11] and monolayer phosphorene [4, 9] obtained by exfoliation. In the case of As, there is a recent study reporting exfoliation of micron-sized flakes of few-layer arsenene (6–12 layers) from gray arsenic (As) [12]. Single-layer arsenene, which is the topic of our paper, was not reported in [12]. Experimental investigations have also been undertaken on antimonene (Sb) [13–15] and bismuthene (Bi) [16]. Extended single layers of antimony and bismuth grown on Ag(1 1 1) and SiC(0 0 0 1), respectively [15, 16], have been interpreted as planar honeycomb structures with significantly larger lattice constants compared to the theoretically predicted buckled structures [7]. There is not yet any experimental report of a single-layer honeycomb structure formed by As, i.e. arsenene. Theoretically, single-layer arsenene prefers a buckled honeycomb structure [17], while puckered [18–21] and planar [18] arsenene are less favorable energetically. The values of the lattice constant (a_{ars}) and the buckling, d, depend on the theoretical method. Values for a_{ars} range from 3.54–3.64 Å [12, 17–19, 21–26, 28–30], and d ranges from 1.35–1.4 Å [12, 17, 21, 23–27, 29, 30]. Arsenene has an indirect gap with calculated values between 1.42 and 1.88 eV when using the Perdew–Burke–Ernzerhof (PBE) functional [12, 18, 19, 21, 22, 24–27, 30] and between 1.72 and 2.49 eV when Heyd–Scurseria–Ernzerhof hybrid functionals (HSE/HSE06) were employed [12, 17–19, 25, 28, 30]. A recent GW_0 calculation resulted in a band gap of 2.75 eV [29]. Strain effects on the electronic structure have been discussed in several papers [17, 19, 23, 25, 28]. Apart from a possible conversion to a direct bandgap semiconductor, strain has also been stud-

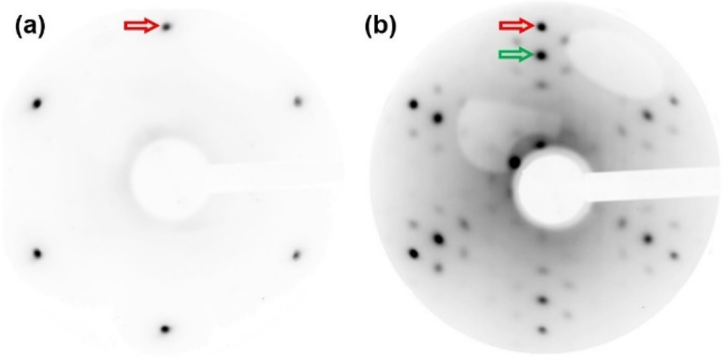

Figure 1. Low-energy electron diffraction. (a) LEED pattern of clean Ag(1 1 1) at 50 eV showing 1 × 1 spots. (b) LEED pattern of arsenene on Ag(1 1 1) at 50 eV. Position of one of the Ag(1 1 1) 1 × 1 spots is indicated by the red arrow, while an arsenene 1 × 1 spot is indicated by the green arrow. LEED pattern corresponds to a 4 × 4 periodicity with respect to the arsenene 1 × 1 structure. Ag(1 1 1) 1 × 1 spots overlap with 4 × spots.

ied as a means to transform arsenene to a topological insulator and to achieve a quantum spin Hall phase [23, 27, 31]. In addition, superconductivity with a transition temperature as high as 30.8 K has been predicted for strained electron-doped arsenene [22]. Other theoretical studies deal with defects in the arsenene layer [21, 32], and the formation of electrical contacts by investigating arsenene metal interfaces [24]. Furthermore, in a theoretical study by Pizzi *et al*, arsenene was identified as a promising 2D material for field effect transistors with application in future nanoelectronics [26].

In this paper, we present evidence of the successful formation of monolayer arsenene on Ag(1 1 1). This conclusion is derived from low-energy electron diffraction (LEED), scanning tunneling microscopy (STM) and angle-resolved photoelectron spectroscopy (ARPES) in combination with density functional theory (DFT) calculations of the atomic and electronic structures. LEED data, shown in figure 1, provide evidence for the formation of a well-ordered As structure. In addition to the 1 × 1 spots from Ag(1 1 1), shown in figure 1(a), several diffraction spots of varying intensity appear after exposure to As.

In particular, there are six bright spots, one of which is indicated by a green arrow in figure 1(b). It is natural to assign these bright spots to diffraction from a 1 × 1 unit cell of the As structure. The diffraction pattern in figure 1(b) can be described as a 4 × 4 periodicity with respect to the ordered As layer. It is worth noting that some of the 4 × spots coincide with 1 × 1 spots of Ag(1 1 1); compare the red arrows in figures 1(a) and (b). From the distances between Ag(1 1 1) 1 × 1 spots in figure 1(a) and distances between As related 1 × 1 spots in figure 1(b), we find that the ratio between the surface lattice constant of Ag(1 1 1) ($a_{\mathrm{Ag111}} = 2.89$ Å) and that of the As structure (a_{ars}) is very close to 0.8. Based on these observations, we can conclude that the As structure has a lattice constant that is $a_{\mathrm{ars}} \approx 1.25 \times 2.89$ Å ≈ 3.61 Å. This experimental value compares very well with theoretical values for the lattice constant of freestanding arsenene, ranging from 3.54–3.64 Å [12, 17–19, 21–26, 28–30]. LEED data clearly indicate that an arsenene layer has formed with the same orientation of the unit cell as that of the Ag(1 1 1) substrate, with a 'perfect' match of $4a_{\mathrm{ars}}$ to $5a_{\mathrm{Ag111}}$. This difference in the lattice constants is the origin of the Moiré type of 4 × 4 LEED pattern observed for arsenene on Ag(1 1 1).

In the following, we present STM and ARPES data, which, in combination with theoretical results, further verify the formation of arsenene.

Arsenene was found to grow uniformly across the Ag(1 1 1) surface. A typical STM image is presented in figure 2(a). This overview shows the arsenene layer on two terraces of the Ag(1 1 1) substrate. The resolution is not sufficient to show the atomic structure, but some typical defects are visible. There are a few dark triangular defects corresponding to missing As atoms. A white arrow in figure 2(a) indicates one such defect. Another type of defect, indicated by a blue arrow, appears as dark lines. These lines have mainly three different orientations, consistent with a hexagonal structure. The zoomed-in image in figure 2(b) reveals the structure responsible for the 4 × periodicity observed by LEED. There is a hexagonal arrangement of rather big bright features separated by a distance corresponding to 4 × a_{ars}. FFTs of STM images such as the one in figure 2(b) show Fourier components that generate a pattern closely matching the diffraction pattern obtained by LEED, see figures 1(b) and 2(c). The line defects in figure 2(b) separate ordered domains of the 4 × structure. There appears to be a small phase shift in the positions of the bright features creating the linear boundaries. However, a detailed structure cannot be derived from figure 2(b). When reducing the bias, the 4 × 4 structure fades out and a 1 × 1 arsenene structure becomes clear, see the inset of figure 2(b). The apparent heights of the As atoms are weakly modulated by the 4 × 4 long-range order originating from the difference in the lattice constants of arsenene and Ag(1 1 1). A

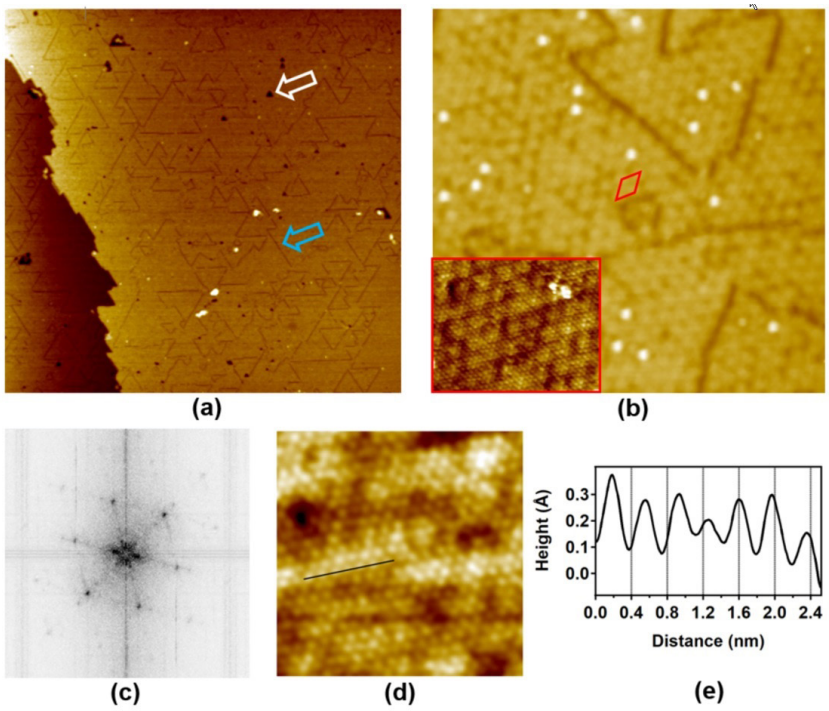

Figure 2. Scanning tunneling microscopy. (a) Filled state (−1 V) STM image, 254 × 254 nm^2. Large-area image shows that the arsenene layer forms uniformly across the surface. White and blue arrows point at two types of defects, i.e. triangular vacancies and straight lines, respectively. (b) Empty state (2 V) STM image, 31 × 31 nm^2 revealing features ordered in a 4 × 4 periodicity, as indicated by the red unit cell. The 4 × 4 features appear much weaker at low bias, as shown by the STM image in the inset (10 meV, 11.7 × 9.2 nm^2). Image shows a hexagonal structure consistent with buckled arsenene as well as the Moiré character of the 4 × 4 periodicity due to the difference in lattice constants between Ag(1 1 1) and arsenene. (c) Representative fast Fourier transform (FFT) of STM images showing 4 × 4 features, as in (b). (d) Atomically resolved empty state (10 mV) STM image, 7.5 × 7.5 nm^2. (e) Line profile along the black line in (d) resulting in an average lattice constant of 3.6 Å, which is consistent with buckled arsenene.

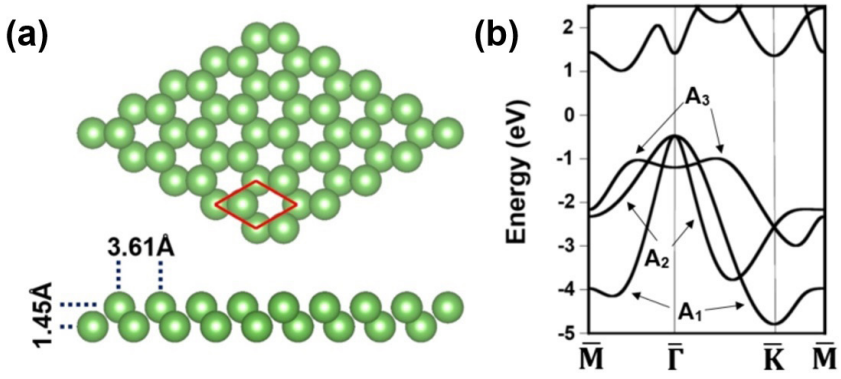

Figure 3. Atomic model and calculated electronic band structure of freestanding arsenene. (a) Top and side views of the arsenene model. (b) Calculated band structure of arsenene. Labels A_1–A_3 have been introduced to facilitate a comparison to experimental bands obtained by ARPES.

hexagonal structure, consistent with the upper sublattice of buckled arsenene, is clearly observed in the STM image in figure 2(d), in which atomic features are well resolved. A value of the lattice constant can be deduced from the topographic profile (figure 2(e)), obtained along the black line in figure 2(d). We find an average value of 3.6 Å, which agrees with the lattice constant derived from LEED.

As a final step to verify the formation of arsenene on Ag(1 1 1), band-structure data from ARPES are compared with the calculated band structure of buckled arsenene. The band structure was calculated from the model in figure 3(a). Using the lattice constant derived from the LEED data, 3.61 Å, resulted in a buckling of 1.45 Å after full relaxation. This value is similar to calculated values in the literature, 1.35 Å [17], 1.38 Å [24] and 1.4 Å [21, 25]. Figure 3(b) shows the band structure along $\bar{M}\bar{\Gamma}\bar{K}\bar{M}$ of the relaxed arsenene structure. As shown by this band structure calculation, arsenene is an indirect bandgap semiconductor. Our calculation results in a gap of 1.47 eV, which falls within the range of the major part of the published values (1.42–1.88 eV [12, 18, 19, 21, 22, 24–27, 30]) using the PBE functional. The three valence bands in figure 3(b) are

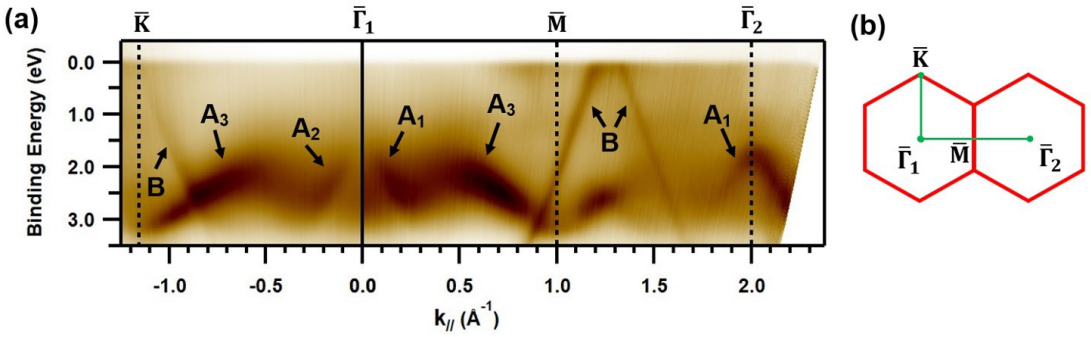

Figure 4. Experimental electronic band structure. (a) Band dispersions obtained by ARPES along $\bar{K}\bar{\Gamma}_1\bar{M}\bar{\Gamma}_2$ of the 1 × 1 surface Brillouin zone (SBZ) of arsenene using a photon energy of 26 eV. A_1, A_2 and A_3 are experimental valence band dispersions. These dispersions closely resemble the calculated bands with the same labels in figure 3(b). B indicates emission from direct transitions between Ag bulk bands. (b) SBZs with symmetry labels and high symmetry lines.

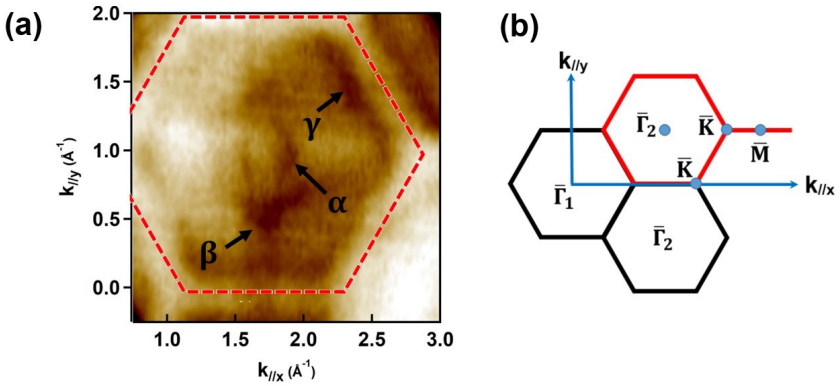

Figure 5. Constant energy contours. (a) Constant energy cut at a binding energy of ≈2.7 eV through a $E(k_x,k_y)$ data set obtained at a photon energy of 130 eV. Three different contours can be identified. There are two partial contours, α, observed mainly horizontally in the figure, and β, mainly observed vertically. Third contour, γ, forms a hexagon close to the SBZ boundary. (b) SBZs of arsenene. $E(k_x, k_y)$ data set was obtained in the SBZ outlined in red centered around $\bar{\Gamma}_2$.

labeled A_1–A_3. These labels are used when discussing the ARPES data presented in figures 4–6.

ARPES data obtained at a photon energy of 26 eV are displayed in figure 4(a). There are several dispersive features along the high symmetry lines of the SBZ indicated in figure 4(b). The features labeled B show the well-known contributions from the Ag substrate originating from direct transitions between Ag bulk bands. All other features correspond to emission from the arsenene layer. Comparing the experimental dispersions with the theoretical bands, we find a close resemblance between the experimental feature A_3 and the calculated band with the same label in figure 3. The experimental dispersion of A_3 follows the periodicity of the arsenene SBZ as verified by the symmetry around the $\bar{M}$-point. Agreement is also found for the steep dispersions observed in the ARPES data close to $\bar{\Gamma}_1$ towards both $\bar{K}$ and $\bar{M}$, which fit with the A_2 and A_1 bands, respectively. It is also important to note that the dispersive band near $\bar{\Gamma}_1$ ($k_{//} = 0$ Å^{-1}), labelled A_1, reappears centered around $k_{//} = 2.0$ Å^{-1}, which corresponds to the distance in k-space between $\bar{\Gamma}_1$ and $\bar{\Gamma}_2$. From this experimental value of the reciprocal lattice dimension, we derive a real space lattice constant of 3.6 Å in agreement with the LEED and STM results.

Proceeding with the comparison, one realizes that the ARPES data show two bands in each of the high symmetry directions, while the calculated band structure has three bands. The A_1 band along $\bar{\Gamma}_1\bar{K}$ and the A_2 band along$\bar{\Gamma}_1\bar{M}$ are not visible in the 26 eV ARPES data in figure 4(a).

An extensive data set in the form of $E(k_x, k_y)$ data was recorded using 130 eV photons in order to verify the existence of all branches of the theoretical band structure in the ARPES data. A constant energy cut at a binding energy of ≈2.7 eV through the ARPES data shows three specific contours that are labeled α, β, and γ, see figure 5(a). The dashed hexagon shows the SBZ as determined from the periodicity of the outer hexagonal contour, γ. The size of the SBZ is consistent with an arsenene lattice constant of 3.6 Å. Figure 5(b) shows the position of the SBZ, from which the ARPES data were obtained, relative to the first SBZ containing the $\bar{\Gamma}_1$ point, This SBZ was chosen since the bands appear more clearly here than in the first SBZ. By comparing these data to the dispersion data in figure 4(a) it is clear that the γ contour corresponds to the A_3 band, while assignments of the α and β contours require further information in terms of $E(k_{//})$ cuts through the data set in figure 5(a). The visibility of the constant

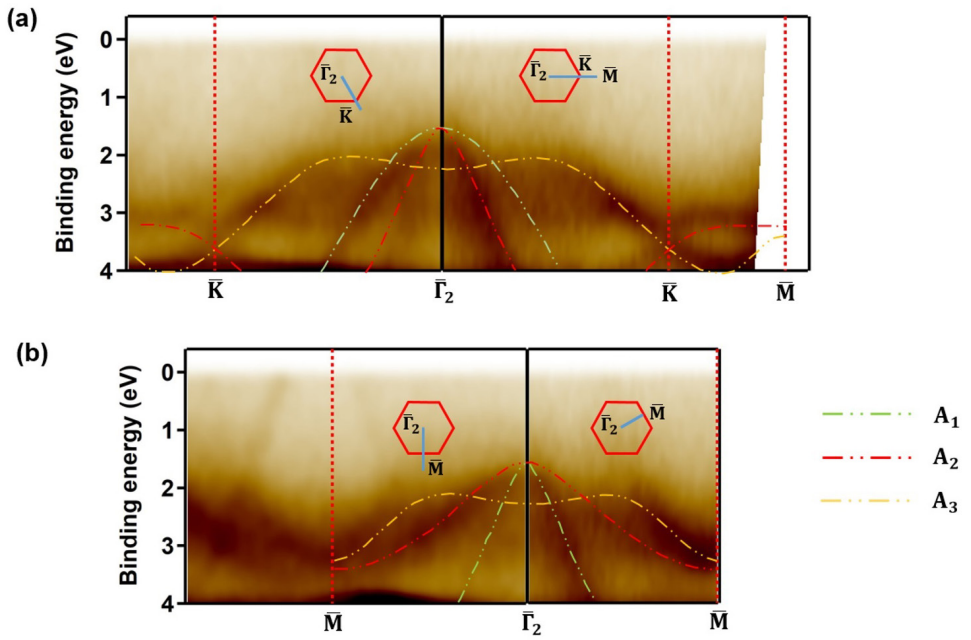

Figure 6. Comparison between experimental and calculated band structures of arsenene. Experimental bands are obtained by cuts through the $E(k_x,k_y)$ data set in figure 5(a). Calculated band structure of arsenene from figure 3(b) is superimposed on the experimental dispersions. A_1, A_2 and A_3 are shown by green, red and yellow dash-dotted lines, respectively. Theoretical bands have been shifted downwards by ~1.0 eV to overlap with the experimental dispersions. (a) Dispersions along $\bar{\Gamma}_2\bar{K}$ obtained in two different directions, as illustrated by the insets in the left- and right-hand parts of the figure. (b) Dispersions along $\bar{\Gamma}_2\bar{M}$ in two different directions, as indicated by the insets. Experimental data in (a) and (b) verify the existence of both A_1 and A_2. A_1 band is observed in the left-hand part of the $\bar{\Gamma}_2\bar{K}$ panel, and A_2 is observed the right-hand part. In the case of $\bar{\Gamma}_2\bar{M}$, A_2 is observed in the left-hand part and A_1 in the right-hand part. There is a very good overall agreement between the experimental and calculated band structures, which is strong evidence for the formation of arsenene.

energy contours varies with the direction in the SBZ. It is therefore necessary to look at more than one $E(k_{//})$ cut to obtain the complete picture of the dispersions along a certain symmetry direction. Figure 6 shows dispersions for two different cuts for each of the $\bar{\Gamma}_2\bar{K}\bar{M}$ and $\bar{\Gamma}_2\bar{M}$ symmetry lines. The fact that these dispersions of the A_1–A_3 bands, obtained at a photon energy of 130 eV, coincide with those obtained by 26 eV photons, verifies the 2D character of the band structure. Figure 6(a) shows experimental dispersions along two $\bar{\Gamma}_2\bar{K}\bar{M}$ directions, as indicated by the inset SBZ figures. Superimposed on the ARPES data is the calculated band structure from figure 3(b). The band structure has the same energy and $k_{//}$ scaling as the experimental data. The absolute energy position has been shifted downwards by about 1.0 eV to obtain a good match with the energy positions of the experimental bands. This implies that the Fermi level of the arsenene layer on the Ag(1 1 1) substrate is located higher by this amount compared to the calculation. One clearly notices that the visibility of the experimental bands differs between the two directions. In the right-hand part of the figure, there is a band with a steep downwards dispersion starting from $\bar{\Gamma}_2$ while in the left-hand part that band is very weak. Instead, another less steep band is observed. Comparing this to the overlaid theoretical band structure, one can conclude that the A_2 band is observed in the right-hand part, while the A_1 band is observed to the left. The dispersions of the A_1 and A_2 bands fit nicely with those of the calculated bands. The experimental bands closest to $\bar{\Gamma}_2$ along $\bar{\Gamma}_2\bar{M}$, shown in figure 6(b), exhibit a similar variation in emission intensity. To the right, the steep A_1 band is observed, while the A_2 band appears in the left-hand part. The dispersion of the third experimental band, A_3, agrees well with the calculated one along both the $\bar{\Gamma}_2\bar{M}$ and $\bar{\Gamma}_2\bar{K}\bar{M}$ symmetry lines of the SBZ. To conclude this comparison, we find that all branches of the calculated band structure are observed in the ARPES data and that experimental band dispersions fit closely with the calculated band structure for freestanding monolayer arsenene. The fact that ARPES shows only three bands is evidence for monolayer arsenene, since the number of bands would increase by three for each additional layer.

In summary, the atomic and electronic structures of a well-ordered As layer on Ag(1 1 1) were experimentally investigated by LEED, STM and ARPES. We have shown that the lattice constant (3.6 Å) and the electron band dispersions of the As layer show close agreement with theoretical results for freestanding buckled arsenene. The fact that ARPES just shows three electron bands is only consistent with the calculated band structure of monolayer arsenene. Altogether, we present strong evidence for the formation of monolayer arsenene with a buckled honeycomb

structure. This finding opens up for investigations of the many interesting properties predicted theoretically for arsenene.

Methods

Experiments

Samples were prepared *in situ* in ultrahigh vacuum systems with base pressures in the 10^{-11} Torr range. The Ag(1 1 1) crystal was cleaned by repeated cycles of sputtering by Ar^+ ions (1 keV) and annealing at approximately 400 °C until a sharp (1 × 1) LEED pattern was obtained. The experimental data in this paper were obtained from arsenene formed on the Ag(1 1 1) substrate by exposure to an As pressure of 2×10^{-7} Torr, while keeping the substrate at 250–350 °C for 3 min. The As pressure was generated by sublimation of As from a heated piece of InAs. The temperature range of 250–350 °C results in a well-defined periodic structure, as evidenced by a sharp 4 × 4 LEED pattern. Extended exposures, both in time and As pressure, do not result in any change in the LEED pattern. The equilibrium vapor pressure for As in the temperature range 250–350 °C is as high as 3×10^{-3}–4×10^{-1} Torr and any buildup of As on the initial layer at the As pressure of 2×10^{-7} Torr is therefore prevented. Annealing of the arsenene layer at 400 °C results in a change to a complex striped phase described by a rectangular $\sqrt{3} \times 14$ unit cell. This sets the upper limit for the substrate temperature for the formation of arsenene. The atomic structure of the $\sqrt{3} \times 14$ phase, as observed by LEED and STM, shows clear similarities with the Ag_2Ge surface alloy reported in the literature [34], which indicates that the amount of As is reduced to 1/3 monolayer.

STM images, recorded at room temperature, using an Omicron variable temperature STM, showed a homogeneous coverage of the substrate by arsenene without any signs of multilayer formation. ARPES data were obtained at room temperature from beamline I4 at MAX-lab (26 eV data) and from the Bloch beamline at MAX IV (130 eV data). A Phoibos 100 analyzer from Specs, with a 2D detector, was used at beamline I4, while a Scienta DA30 analyzer was used at the Bloch beamline. The energy and angular resolutions were 50 meV and 0.3°, respectively.

Calculations

DFT calculations were performed to investigate the band structure of freestanding monolayer arsenene. A slab model was used where consecutive slabs, consisting of a buckled arsenene layer with a lattice constant of 3.61 Å, were separated by 19 Å of vacuum to avoid interaction between the slabs. All atoms were relaxed until the average force was within 0.01 eV $Å^{-1}$. The band structure was calculated using the PBE functional and the projector augmented wave method Vienna *ab initio* simulation package code [33]. The energy cutoff of the plane-wave basis set was 434 eV, and the *k*-point mesh was (9 × 9 × 1).

Acknowledgments

Technical support from Dr Johan Adell, Dr Craig Polley and Dr T Balasubramanian at MAX-lab is gratefully acknowledged. Financial support was provided by the Swedish Research Council (Contract No. 621-2014-4764) and by the Linköping Linnaeus Initiative for Novel Functional Materials supported by the Swedish Research Council (Contract No. 2008-6582). The calculations were carried out at the National Supercomputer Centre (NSC), supported by the Swedish National Infrastructure for Computing (SNIC).

We acknowledge MAX IV Laboratory for time on Beamline Bloch under Proposals 20190001 and 20190210. Research conducted at MAX IV, a Swedish national user facility, is supported by the Swedish Research council under contract 2018-07152, the Swedish Governmental Agency for Innovation Systems under contract 2018-04969, and Formas under contract 2019-02496.

ORCID iDs

W Wang https://orcid.org/0000-0002-1036-070X

References

[1] Geim A K and Novoselov K S 2007 The rise of graphene *Nat. Mater.* **6** 183
[2] Castro Neto A H, Guinea F, Peres N M R, Novoselov K S and Geim A K 2009 The electronic properties of graphene *Rev. Mod. Phys.* **81** 109
[3] Krawiec M 2018 Fuctionalization of group-14 two-dimensional materials *J. Phys.: Condens. Matter* **30** 233003 (references therein.)
[4] Liu H, Neal A T, Zhu Z, Luo Z, Xu X, Tománek D and Ye D P 2014 Phosphorene: an unexplored 2D semiconductor with a high hole mobility *ACS Nano* **8** 4033
[5] Wang C, Xia Q, Nie N and Guo G 2015 Strain-induced gap transition and anisotropic Dirac-like cones in monolayer and bilayer phosphorene *J. Appl. Phys.* **117** 124302
[6] Liang L, Wang J, Lin W, Sumpter B G, Meunier V and Pan M 2014 Electronic bandgap and edge reconstruction in phosphorene materials *Nano Lett.* **14** 6400
[7] Zhang S, Xie M, Li F, Yan Z, Li Y, Kan E, Liu W, Chen Z and Zeng H 2016 Semiconducting group 15 monolayers: a broad range of band gaps and high carrier mobilities *Angew. Chem., Int. Ed.* **55** 1666
[8] Tran V, Soklaski R, Liang Y and Yang L 2014 Layer-controlled band gap and anisotropic excitons in a few-layer black phosphorus *Phys. Rev.* B **89** 235319
[9] Wang X, Jones A M, Seyler K L, Tran T, Jia Y, Zhao H, Wang H, Yang L, Xu X and Xia F 2015 Highly anisotropic and robust excitons in monolayer black phosphorus *Nat. Nanotechnol.* **10** 517

[10] Li L, Yu Y, Ye G J, Ge Q, Ou X, Wu H, Feng D, Chen X H and Zhang Y 2014 Black phosphorous field-effect transistors *Nat. Nanotechnol.* **9** 372
[11] Xia F, Wang H and Jia Y 2014 Rediscovering black phosphorus as an anisotropic layered material for optoelectronics and electronics *Nat. Commun.* **5** 4458
[12] Vishnoi P, Mazumder M, Pati S K and Rao C N R 2018 Arsenene nanosheets and nanodots *New J. Chem.* **42** 14091
[13] Ji J *et al* 2016 Two-dimensional antimonene single crystals grown by van der Waals epitaxy *Nat. Commun.* **7** 13352
[14] Fortin-Deschênes M, Waller O, Mentes T O, Locatelli A, Mukherjee S, Genuzio F, Levesque P L, Hébert A, Martel R and Moutanabbir O 2017 Synthesis of antimonene on germanium *Nano Lett.* **17** 4970
[15] Shao Y *et al* 2018 Epitaxial growth of flat antimonene monolayer: A new honeycomb analogue of graphene *Nano Lett.* **18** 2133
[16] Reis F, Li G, Dudy L, Bauernfeind M, Glass S, Hanke W, Thomale R, Schäfer J and Claessen R 2017 Bismuthene on a SiC substrate: a candidate for a high-temperature quantum spin Hall material *Science* **357** 287
[17] Zhang S, Yan Z, Li Y, Chen Z and Zeng H 2015 Atomically thin arsenene and antimonene: semimetal-semiconductor and indirect-direct-gap transitions *Angew. Chem.* **127** 3155
[18] Kamal C and Ezawa M 2015 Arsenene: two dimensional buckled and puckered honeycomb arsenic systems *Phys. Rev.* B **91** 085423
[19] Zhu Z, Guan J and Tománek D 2015 Strain-induced metal-semiconductor transition in monolayers and bilayers of gray arsenic: a computational study *Phys. Rev.* B **91** 161404
[20] Wang C, Xia Q, Nie N, Rahman M and Guo G 2016 Strain engineering band gap, effective mass and anisotropic Dirac-like cone in monolayer arsenene *AIP Adv.* **6** 035204
[21] Iordanidou K, Kioseoglou J, Afanas'ev V V, Stesmans A and Houssa M 2017 Intrinsic point defects in buckled and puckered arsenene: a first principles study *Phys. Chem. Chem. Phys.* **19** 9862
[22] Kong X, Gao M, Yan X-W, Lu Z-Y and Xiang T 2018 Superconductivity in electron-doped arsenene *Chin. Phys.* B **27** 046301
[23] Wang Y-P, Zhang C-W, Ji W-X, Zhang R-W, Li P, Wang P-J, Ren M-J, Chen X-L and Yuan M 2016 Tunable quantum spin Hall effect via strain in two-dimensional arsenene monolayer *J. Phys. D: Appl. Phys.* **49** 055305
[24] Wang Y *et al* 2017 Electrical contacts in monolayer arsenene devices *ACS Appl. Mater. Interfaces* **9** 29273
[25] Kou L, Ma Y, Tan X, Frauenheim T, Du A and Smith S 2015 Structural and electronic properties of layered arsenic and antimony arsenide *J. Phys. Chem.* C **119** 6918
[26] Pizzi G, Gibertini M, Dib E, Marzari N, Iannaccone G and Fiori G 2016 Performance of arsenene and antimonene double-gate MOSFETs from first principles *Nat. Commun.* **7** 12585
[27] Wang Y-P, Ji W-X, Zhang C-W, Li P, Li F, Ren M-J, Chen X-L, Yuan M and Wang P-J 2016 Controllable band structure and topological phase transitions in two-dimensional hydrogenated arsenene *Sci. Rep.* **6** 20342
[28] Sharma S, Kumar S and Schwingenschlögl U 2017 Arsenene and antimonene: two-dimensional materials with high thermoelectric figures of merit *Phys. Rev. Appl.* **8** 044013
[29] Yu J, Katsnelson M I and Yaun S 2018 Tunable electronic and magneto-optical properties of monolayer arsenene: from GW_0 approximation to large-scale tight-binding propagation simulations *Phys. Rev.* B **18** 115117
[30] Jamdagni P, Thakur A, Kumar A, Ahluwalia P K and Pandey R 2018 Two dimensional allotropes of arsenene with a wide range of high and anisotropic carrier mobility *Phys. Chem. Chem. Phys.* **20** 29939
[31] Zhang H, Ma Y and Chen Z 2015 Quantum spin Hall insulators in strain-modified arsenene *Nanoscale* **7** 19152
[32] Sun X, Liu Y, Song Z, Li Y, Wang W, Lin H, Wang L and Li Y 2017 Structures, mobility and electronic properties of point defects in arsenene, antimonene and an antimony alloy *J. Mater. Chem.* C **5** 4159
[33] Kresse G and Joubert D 1999 From ultrasoft pseudopotentials to the projector augmented-wave method *Phys. Rev.* B **59** 1758
[34] Wang W, Sohail H M, Osiecki J R and Uhrberg R I G 2014 Broken symmetry induced band splitting in the Ag_2Ge surface alloy on Ag(111) *Phys. Rev.* B **89** 125410